Quantum Simulation of a Hydrated Noradrenaline Analog with the Torsional Path Integral Method†

Thomas F. Miller III and David C. Clary*

Physical and Theoretical Chemistry Laboratory, Oxford University, South Parks Road, Oxford OX1 3QZ, U.K.

Received: September 9, 2005; In Final Form: November 9, 2005

An extended version of the torsional path integral Monte Carlo (TPIMC) method is presented and shown to be useful for studying the conformation of flexible molecules in solvated clusters. The new technique is applied to the hydrated clusters of the 2-amino-1-phenyl-ethanol (APE) molecule. APE + $n$$H_2O$ clusters with $n = 0-4$ are studied at 100 and 300 K using both classical and quantum simulations. Only at the lower temperature is the hydration number n found to impact the conformational distribution of the APE molecule. This is shown to be a result of the temperature-dependent balance between the internal energy and entropy contributions to the relative conformer free energies. Furthermore, at 100 K, large quantum effects are observed in the calculated conformer populations. A particularly large quantum shift of 30% of the total population is calculated for the APE + $2H_2O$ cluster, which is explained in terms of the relative zero point energy of the lowest-energy hydrated structures for this cluster. Finally, qualitative agreement is found between the reported calculations and recent spectroscopy experiments on the hydrated clusters of APE, including an entropically driven preference for the formation of AG-type hydrated structures and the formation of a water "droplet" in the APE + $4H_2O$ cluster.

I. Introduction

Determining the conformation of small, biologically active molecules is a topical problem in physical chemistry.[1,2] The conformational preference of such molecules is related to the strength and specificity with which they noncovalently bind at receptor sites, which in turn affects their biological function.[3,4]

However, the determination of molecular conformation poses serious challenges for both theory and experiment. Small biomolecules are often highly flexible, exhibiting a multitude of energetically competitive conformations.[5−10] The relative populations of these conformations are delicately balanced and sensitive to a variety of external factors, including temperature and the presence and identity of solvent molecules. Theoretical predictions of molecular conformation can suffer from unrealistic descriptions of these external factors or inaccurate potential energy surfaces. Experimental determinations are complicated by the difficulty of distinguishing between conformers and uncertainties in the experimental conditions (i.e., whether thermal equilibrium has been established).

Developments in gas phase spectroscopy have greatly improved the ability of experimentalists to investigate the conformation of isolated biomolecules and their solvated clusters.[11−17] For example, the combination of resonant 2-photon ionization (R2PI) spectroscopy with time-of-flight mass spectrometry (TOF−MS) enables the mass-selection of clusters with a desired number of solvent molecules. Furthermore, spectral hole-burning techniques, such as resonant ion−dip infrared spectroscopy, probe the various conformations exhibited by a particular cluster. These techniques have made the investigation of biomolecular conformation increasingly feasible and reliable, although many such experiments remain heavily dependent on computational results for their interpretation.

The most commonly employed theoretical methods for the study of molecular conformation of gas-phase biomolecules and their solvated clusters are (1) electronic structure theory or molecular mechanics calculations with thermodynamic corrections based on harmonic vibrational frequency calculations and (2) classical molecular dynamics (MD) simulations. The first approach can provide a high-level description of the relative electronic energies of the various conformers. However, it neglects the anharmonicity of the potential energy surface, to which the thermodynamics of isolated, flexible molecules is very sensitive.[18−25] This problem only gets worse in the context of clusters with weakly bound solvent molecules.[26−30] The second approach, classical MD simulation, provides a fully anharmonic description of the potential energy surface, but it fails to account for quantum mechanical effects in the nuclear motion. Such effects, including quantum zero point energy, have been shown to cause large changes in the conformational distribution of hydrogen-bonded systems.[24−26,30]

In a series of recent articles, we have developed the torsional path integral Monte Carlo (TPIMC) method to study both anharmonic and quantum mechanical effects in the conformational thermodynamics of isolated biomolecules.[23−25,31−34] In applications to the 2-amino-1-phenyl-ethanol (APE) molecule and the glycine amino acid, the TPIMC method treats anharmonicity in the potential energy surface to yield good agreement with experimentally obtained conformer populations at a variety of temperatures.[24,25] We extend the TPIMC method in the current study to explore the effects of explicit solvation on the conformational preference of the APE molecule. This molecule, shown schematically in Figure 1, is a structural analogue of the neurotransmitter noradrenaline and the prototype molecule of the pharmaceutically relevant ephedrine series.[35−37]

† Part of the special issue "Donald G. Truhlar Festschrift".

10.1021/jp055108l CCC: $33.50
Published on Web 12/14/2005

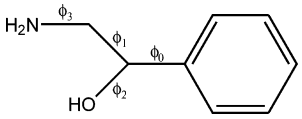

Figure 1. Schematic of the APE molecule with torsional angles labeled.

II. Methodology

Since a detailed description of the TPIMC method for isolated molecules is available elsewhere,[31,32] only a summary of the approach is included here. The intramolecular Hamiltonian of a flexible molecule is approximately expressed in terms of the torsional degrees of freedom,

$$H_{\mathrm{tor}} = \sum_{i=1}^{M} \frac{-\hbar^2}{2I_i} \frac{\partial^2}{\partial \phi_i^2} + V(\vec{\phi}) \tag{1}$$

where M is the number of intramolecular torsions, I_i is the moment of inertia corresponding to the torsional angle ϕ_i, and the potential $V(\vec{\phi})$ is a coupled function of the torsional coordinates that is obtained from either electronic structure theory calculations or a molecular mechanics force field. The quantum statistical mechanics of this Hamiltonian are then expressed in the path integral representation[38,39]

$$Q(P,\beta) = \int \mathrm{d}\vec{\phi}\, \rho^{\mathrm{tor}}(\vec{\phi}) f(V(\vec{\phi})) \tag{2}$$

where[31,40,41]

$$\rho^{\mathrm{tor}}(\vec{\phi}) = \left(\frac{P}{2\pi\beta\hbar^2}\right)^{MP/2} \left(\prod_{i=1}^{M} I_i\right)^{P/2} \exp\left(-\frac{P}{2\beta\hbar^2} \sum_{t=1}^{P} \sum_{i=1}^{M} I_i (\phi_i^{(t)} - \phi_i^{(t+1)})\right) \tag{3}$$

and

$$f(V(\vec{\phi})) = \exp\left(-\frac{\beta}{P} \sum_{t=1}^{P} V(\vec{\phi}^{(t)})\right) \tag{4}$$

In these expressions, P is a parameter indicating the number of Trotter beads in the path integral representation, $\beta = (k_{\mathrm{B}}T)^{-1}$ is the reciprocal temperature of the simulation, and the notation $\phi_i^{(t)}$ refers to the coordinate for the ith torsion of the tth Trotter bead.

The quantum partition function thus assumes the form of a classical configuration integral of dimension $M \times P$, which may be evaluated using standard Monte Carlo techniques.[42] For sufficiently large values of P, $Q(P,\beta)$ converges to the exact quantum canonical partition function and the normalized integrand converges to the quantum mechanical Boltzmann probability distribution. Alternatively, when the parameter P is set to 1, then $\rho^{\mathrm{tor}}(\vec{\phi}) = 1$, $f(V(\vec{\phi})) = \exp(-\beta V(\vec{\phi}))$, and the familiar expression for the classical canonical partition function is obtained.

The TPIMC method is appealing in several regards. First, like many path integral methods, it provides a straightforward framework in which to examine the effects of quantum mechanics on the intramolecular partition function. Second, unlike conventional path integral approaches that explicitly treat all intramolecular degrees of freedom, the TPIMC expression for the canonical partition function converges to the quantum limit with only a very small number of Trotter beads (typically $P = 3-5$), which greatly reduces its computational cost. Finally, since the TPIMC method only explicitely treats the low-frequency torsional motions, computational effort is focused on a high-quality description of the degrees of freedom to which the conformer free energies are especially sensitive. Thermodynamic contributions from the nontorsional modes can then be included using simple harmonic corrections,[23,34] or they can be adiabatically included in the torsional Hamiltonian.

Previous applications of the TPIMC method have addressed only isolated biomolecules in the gas phase. In the current paper, we consider the more complicated case of a biomolecule in a hydrated cluster. Therefore, in addition to the intramolecular degrees of freedom of the flexible biomolecule, we shall have to describe the motion of the molecules in the cluster with respect to each other. These essential features of the hydrated cluster are captured in the following Hamiltonian:

$$H_{\mathrm{cluster}} = \sum_{i=1}^{M} \frac{-\hbar^2}{2I_i} \frac{\partial^2}{\partial \phi_i^2} - \sum_{j=1}^{n} \sum_{k=1}^{3} \frac{\hbar^2}{2m} \frac{\partial^2}{\partial r_{jk}^2} + \sum_{j=1}^{n} \sum_{l=1}^{3} \frac{1}{2\omega_l} \hat{J}_{jl}^2 + V(\vec{\phi},\vec{\vec{r}},\vec{\vec{\theta}}) \tag{5}$$

The first term in eq 5 is immediately recognizable as the kinetic energy contribution of the M torsions in the flexible biomolecule. The second and third terms respectively correspond to the rigid body translation and rotation of the n water molecules in the hydrated cluster. Specifically, r_{jk} is the center of mass position of the jth water molecule along the lth laboratory-frame axis, m is the total mass of each water molecule, $\hat{J}_{jl}$ is the angular momentum operator for the rotation of the jth water molecule about its lth principle-axis, and ω_l is the corresponding principal axis moment of inertia. The last term in eq 5 is the potential energy, a coupled function of the torsional, translational, and orientational coordinates.

The path integral representation for the quantum mechanical partition function of the Hamiltonian in eq 5 can be written

$$Q(P,\beta) = \int \mathrm{d}\vec{\phi} \int \mathrm{d}\vec{\vec{r}} \int \mathrm{d}\vec{\vec{\theta}}\, \rho^{\mathrm{tor}}(\vec{\phi}) \rho^{\mathrm{trans}}(\vec{\vec{r}}) \rho^{\mathrm{rot}}(\vec{\vec{\theta}}) f(V(\vec{\phi},\vec{\vec{r}},\vec{\vec{\theta}})) \tag{6}$$

With the use of existing path integral techniques, each term in the integrand is easily evaluated. The function ρ^{tor} is unchanged from eq 3, ρ^{trans} follows from the well-known primitive path integral representation of translational motion,[39] ρ^{rot} can be calculated using a method by Kuharski and Rossky that is based on the fixed-axis approximation,[43] and the functional $f(V)$ is also unchanged from eq 4.

Equation 6 is a $(M + 6n) \times P$ dimensional integral that can be evaluated using standard Monte Carlo techniques. It converges to the exact quantum partition function for the hydrated cluster Hamiltonian with sufficiently large values of P, and for $P = 1$, the exact classical partition function is obtained. The integrand

$$\rho(\vec{\phi},\vec{\vec{r}},\vec{\vec{\theta}}) = \rho^{\mathrm{tor}}(\vec{\phi}) \rho^{\mathrm{trans}}(\vec{\vec{r}}) \rho^{\mathrm{rot}}(\vec{\vec{\theta}}) f(V(\vec{\phi},\vec{\vec{r}},\vec{\vec{\theta}})) \tag{7}$$

is the path integral representation of the Boltzmann probability distribution for the coordinates of the hydrated cluster.

Equation 6 is a natural extension of the TPIMC technique. It provides a framework in which to perform both quantum mechanical and classical mechanical simulations of the hydrated cluster, and it addresses the low-frequency motions that are essential for describing the conformational preference of the hydrated biomolecule. Furthermore, since the majority of quantum effects in the rotation and translation of rigid water

TABLE 1: Relative ab Initio and MM3 Potential Energies for the Most Stable Conformers of the Unhydrated APE Molecule

	AG1	AG2	AG2′	GG1	GG2	GG2′
ab initio[a]	0.6	7.7	8.4	0.0	6.1	
MM3[b]	0.0	7.4	4.7	0.7	6.4	10.0

[a] E_{ZP} in kJ/mol. MP2/6-311G**//MP2/6-31G* relative electronic energies corrected with HF/6-31G* zero-point harmonic vibrational energies.[8] [b] E_{ZP} in kJ/mol. MM3 relative electronic energies corrected with torsional MM3 zero-point harmonic vibrational energies.

are recovered with a small number of Trotter beads,[43] the value of P needed to converge the quantum description of the hydrated biomolecule is no larger than that needed in the unhydrated calculation.

Before proceeding, we note that eq 6 neglects the rotational and translational motion of the flexible biomolecule. This is a reasonable first approximation, since the biomolecule is generally much heavier than the surrounding waters and will move slowly in comparison. However, if it is assumed that the rotational moments of inertia for the biomolecule do not change as a function of its torsional coordinates, eq 6 can be trivially extended to include the rotational and translational motion of the biomolecule. This has been done for the calculations presented in the current study.

III. Computational Details

Using the extended TPIMC method described in section II, we have studied the explicit solvation of the APE molecule at 100 and 300 K. We have considered the unhydrated APE molecule and its four smallest hydrated clusters (APE + nH$_2$O, where $n = 0, ..., 4$). The integer n, which specifies the number of water molecules in the cluster, will be referred to as the hydration number.

Two simulations were performed for each hydrated cluster: Classical results were obtained from a TPIMC simulation using one Trotter bead ($P = 1$), and quantum results were obtained from a TPIMC simulations using three Trotter beads ($P = 3$). Monte Carlo importance sampling of the Boltzmann distribution in eq 7 was performed with parallel tempering at 100, 125, 150, 200, 250, 300, 375, 450, and 600 K.[23,42] Each calculation included at least five independent runs of at least 5×10^7 Monte Carlo steps, and data samples were collected at every 20 steps to reduce correlation. Configuration step sizes were adjusted to ensure approximately 50% acceptance with the Metropolis algorithm, and the fraction of attempted parallel tempering "swapping" moves was chosen to be between 25% and 40%. For all calculations, the estimator bias was found to be within the standard deviation of the reported result.

Although the TPIMC technique may be employed using any potential energy surface, the MM3 molecular mechanics potential was selected for this study because of its good agreement with previously published ab initio calculations for the unhydrated APE molecule.[44] Graham et al. have reported the relative APE potential energies at the MP2/6-311G**//MP2/6-31G* level of theory with HF/6-31G* harmonic zero-point vibrational corrections.[8] For the most stable conformers of the unhydrated APE molecule, Table 1 shows that the ab initio and MM3 relative energies agree to within the expected accuracy of the ab initio calculations. Furthermore, the MM3 potential energy for the global minimum of the water dimer relative to that of the separated monomers is 4.8 kcal/mol, which is consistent with high-level ab initio calculations.[45]

The bond lengths and angles used to define the nontorsional structure of the APE molecule during the TPIMC simulations were chosen to be the average of the values obtained from geometry optimizations of the AG1 and GG1 conformations using the MM3 potential. For all six APE conformers considered in Table 1, the averaged structure differs from the fully relaxed conformer geometry by less than 0.002 Å for each bond length and 1.1 ° for each bond angle. Furthermore, the averaged structure changed the relative energy of the dominant AG1 and GG1 conformers by less than 0.04 kJ/mol. The geometry utilized for the rigid water molecules was that of the optimized structure on the MM3 potential energy surface.

Although the MM3 prediction of the binding energy for a water molecule to the APE molecule (approximately 5 kcal/mol, depending on the conformation) exceeds the average translational energy of the molecules at the temperatures considered in this chapter, the following constraint potential was utilized to prevent the water molecules dissociating from the hydrated clusters during the TPIMC simulations,

$$V_{\text{constr}} = \sum_{i=1}^{N} A\left(\frac{R_i}{R^{\text{c}}}\right)^{32} \tag{8}$$

where the parameter A is set to 1 kcal/mol, R^{c} is 12 Å, and R_i is the distance between the center-of-mass of the APE molecule and the ith water molecule. The function in eq 8 does not affect the potential energy except at geometries well away from equilibrium. Constraining potentials of this sort are regularly employed in the simulation of weakly bound clusters.[46−48]

For the unhydrated molecule, separate simulations performed using three and five Trotter beads showed no significant differences in the conformer populations calculated at 100 and 300 K. Furthermore, Kuharski and Rossky showed that the vast majority of quantum effects in the static properties of liquid water at room temperature were recovered using only $P = 3$.[43] It is therefore reasonable to assume that the majority of quantum effects in the hydrated clusters of the APE molecule will be described in our simulations.

The thermodynamic contribution from nontorsional vibrations is only implicitly included for the TPIMC calculations reported in this paper. This involves two primary assumptions: (1) The nontorsional contributions are assumed to be adiabatically included in the potential energy surface, which is supported in the limit of 0 K by the results shown in Table 1. (2) The relative nontorsional contributions are assumed to be independent of temperature, which is supported by the fact that the nontorsional modes are generally higher in frequency than the torsional modes and are thus less likely to be thermally populated. More sophisticated treatments of the nontorsional vibrations are discussed elsewhere.[23,34]

IV. Results and Discussion

Reduced torsional probability distributions provide a useful means of visualizing the conformational distribution of the APE molecule in its various hydrated clusters. For each cluster, the path integral representation of the Boltzmann probability distribution, $\rho(\vec{\phi},\vec{r},\vec{\theta})$ (eq 7), is a function of the four torsional coordinates of the APE molecule ($\vec{\phi} = \{\phi_0,\phi_1,\phi_2,\phi_3\}$), the translational coordinates of the APE and the water molecules (collectively represented as $\vec{r}$), and the rotational coordinates of the APE and the water molecules (collectively represented as $\vec{\theta}$). Integrating this multidimensional function over the rotational and translational coordinates yields the torsional probability distribution $\rho(\vec{\phi})$, which can be further integrated to yield reduced torsional distributions and the hydrated APE conformer populations.

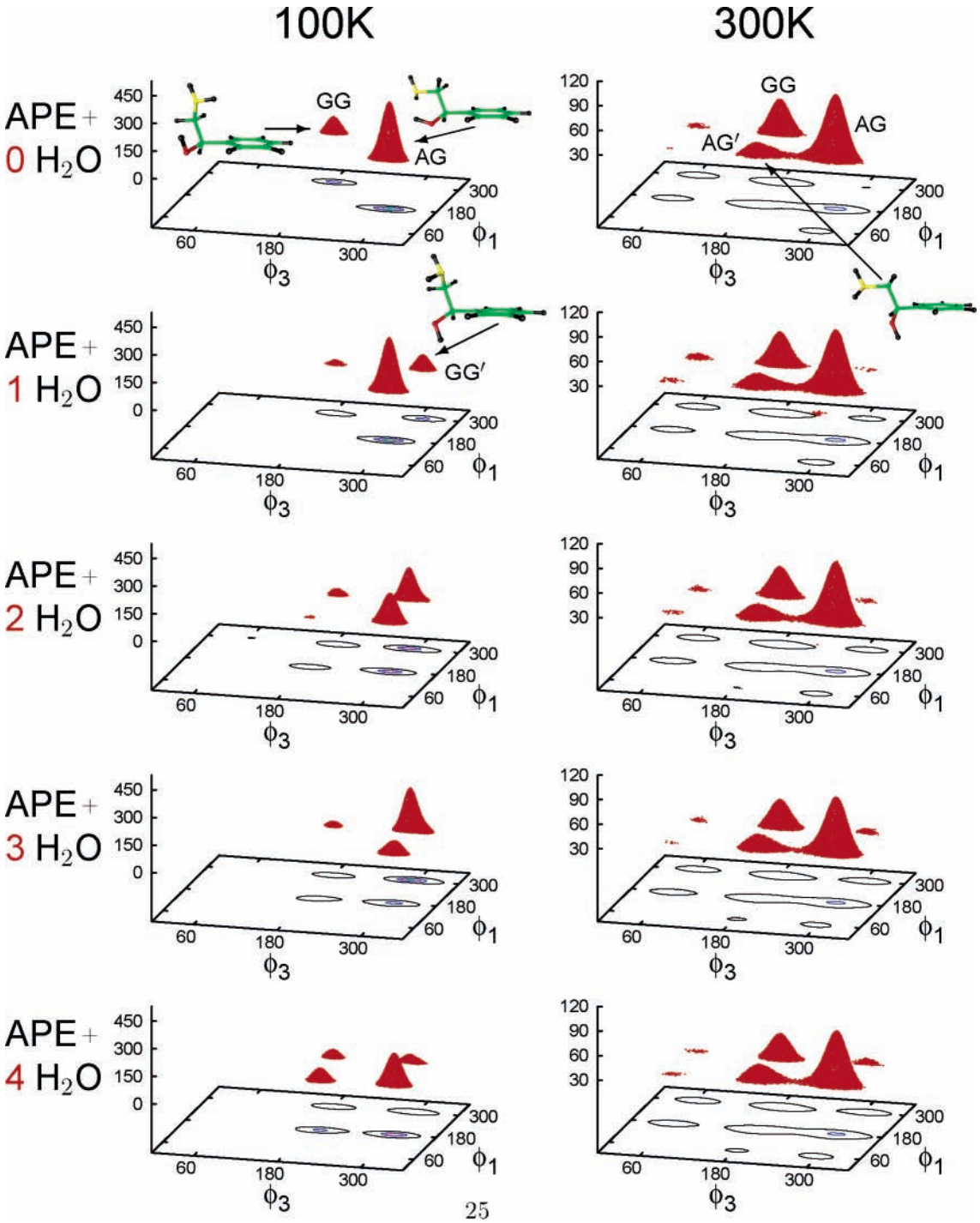

Figure 2. Probability distributions for the hydrated APE clusters as a function of the backbone C−C torsion ϕ_1 and the $-NH_2$ torsion ϕ_3. The distribution plots calculated at 100 K (left column) show a strong dependence on the number of water molecules in the cluster, whereas the distributions calculated at 300 K (right column) do not.

Figure 2 presents reduced torsional distributions obtained from the quantum TPIMC simulations of the various hydrated clusters at 100 and 300 K. The columns in the figure correspond to the different simulation temperatures and the rows correspond to the different hydration numbers. These probability distributions, which were obtained by integrating $\rho(\phi)$ over the phenyl torsion $\phi_0 \in [0°,360°]$ and the −OH torsion $\phi_2 \in [0°,360°]$, display the distribution of the population of the hydrated APE molecule as a function of the backbone C−C torsion ϕ_1 and the $-NH_2$ torsion ϕ_3.

The top-left plot in Figure 2 displays the torsional distribution of the unhydrated APE molecule at 100 K. The results for this particular calculation are familiar from ref 24; the two peaks in the torsional distribution correspond to the AG1 conformer at $(\phi_1,\phi_3) = (180°,300°)$ and the GG1 conformer at $(\phi_1,\phi_3) = (300°,180°)$. The AG1:GG1 population ratio obtained from integrating these two peaks is 3.98(6), which is entirely consistent with the quantum TPIMC result at 100 K presented in ref 24.

Note that the APE conformer labels shown in Figure 2 (AG, GG′, etc.) are less specific than those employed in previous studies[8,24] (AG1, GG2′, etc.). The nomenclature employed for the remainder of the current study, which is defined in Table 2, does not specify the orientation of the −OH torsion, ϕ_2. This

TABLE 2: Torsional Angle Ranges for the Hydrated APE Conformers

	ϕ_0	ϕ_1	ϕ_2	ϕ_3
AG	[0°,360°]	[120°,240°]	[0°,360°]	[240°,360°]
AG′	[0°,360°]	[120°,240°]	[0°,360°]	[120°,240°]
GG	[0°,360°]	[240°,360°]	[0°,360°]	[120°,240°]
GG′	[0°,360°]	[240°,360°]	[0°,360°]	[240°,360°]

was found to be more convenient for the discussion of the hydrated APE clusters.

1. Temperature and Hydration Number Dependence. Figure 2 illustrates the effects of temperature and hydration number on the torsional distribution of the APE molecule. The conformer populations obtained by integrating these distribution plots are reported in Table 3.

The plots in the left column of Figure 2 reveal that at 100 K, changes in the hydration number n of the APE + nH$_2$O clusters give rise to substantial shifts in the torsional distribution. For the unhydrated cluster, it was previously noted that only the AG and GG conformers are substantially populated. However, the addition of a water molecule ($n = 1$) causes 20% of the torsional distribution to shift to the GG′ conformer. A second water molecule increases the GG′ population to 40%, and a third further increases it to 60%. Finally, the addition of a fourth water molecule reverses this trend as 45% of the total conformer population shifts from the GG′ conformer to the AG and AG′ conformers.

The plots in the right column of Figure 2 reveal strikingly different behavior at 300 K. No substantial changes in the torsional distribution are observed upon changing the hydration number; the conformer populations for the hydrated clusters are virtually indistinguishable from that of the unhydrated cluster. This result is further illustrated by the conformer populations reported at 300 K in Table 3.

We have seen in Figure 2 and Table 3 that the APE conformer populations are strongly dependent on the hydration number at low temperature and weakly dependent on the hydration number at high temperature. To explain the difference in these trends, we will consider the relative internal energies and entropies of the APE conformers. The relative internal energies $\Delta E°$ are directly calculated in the TPIMC simulations,[49] and the relative entropies $\Delta S°$ are obtained from the thermodynamic relationship[50]

$$\Delta A° = \Delta E° - T\Delta S° \tag{9}$$

where the relative free energies $\Delta A°$ are obtained from the ratio of the conformer populations K_{eq} via

$$K_{eq} = e^{-\beta\Delta A°} \tag{10}$$

At low temperature, it is clear from eq 9 that the relative conformer free energies (and hence the relative conformer populations) are dominated by the internal energy term. Therefore, although the calculated values for $\Delta E°$ and the $\Delta S°$ are not strongly dependent on the temperature of the simulations, the trends in Figure 2 are best explained in terms of the $\Delta E°$ calculated at 100 K and the $\Delta S°$ calculated at 300 K. These results are provided in Table 4.

There is clearly a strong correlation between the relative internal energy of the conformers (Table 4) and their relative population at 100 K (Table 3). For the unhydrated cluster ($n = 0$), the AG and GG conformers have the lowest internal energies and are the only populated conformers. For the hydrated clusters with $n = 1-3$, the internal energy of the GG′ conformer drops substantially with respect to that of the other conformers, which coincides with marked increases in the GG′ conformer population. Finally, for $n = 4$, the internal energies of all four conformers are calculated to very similar, which is consistent with the even distribution of APE conformer populations found for this particular cluster.

Further comparison of the calculated conformer populations in Table 3 with the thermodynamic results in Table 4 confirms that entropy plays a more important role at 300 K. Consider, for example, the relative population of the AG′ and GG′ conformers for the hydrated cluster with $n = 1$. At 100 K, we have seen that the GG′ conformer is much more populated because of its lower internal energy. However, the AG′ conformer is entropically favored by approximately 35 J/mol/K, so that increasing the temperature from 100 to 300 K causes the free energy of AG′ conformer to drop by 7 kJ/mol with respect to that of the GG′ conformer. The result is a strong temperature dependence in the relative population of these two conformers. The same effect is seen in the hydrated clusters with $n = 2$ and $n = 3$.

Table 4 also shows that the relative conformer entropies are calculated to be substantially less dependent on the hydration number than the relative internal energies. The relative conformer internal energies rise and fall with each additional water molecule, but the relative internal entropies (with the exception of that of the unhydrated GG′ conformer) are generally less variant. This can be understood as follows: The internal energies are sensitive to the potential energy of individual structures, which depend on the number of water molecules and the specific geometry in which they bind to each other and the APE molecule. However, the entropies only depend on the total number of energetically accessible structures, which will consistently be larger for some APE conformers, regardless of the number of water molecules present.

The conclusions from Table 4 can now be used to explain the trends observed in Figure 2. The strong correlation between the APE conformer populations and the hydration number at 100 K is due to the fact that at low temperature, the relative conformer free energies are dominated by the relative internal energies, which we have calculated to be strongly dependent on hydration number. However, at higher temperatures, a larger component of the relative free energies corresponds to the relative conformer entropies, which we have calculated to be less dependent on the hydration number. The subtle details of the potential energy surface of the hydrated APE clusters that are important at 100 K simply get washed out at 300 K.

2. Quantum Effects. Table 5 offers an indication of the degree to which quantum effects alter the conformer populations of the hydrated APE molecule. It reports the difference between the conformer populations obtained in the separate classical and quantum TPIMC simulations. As might be expected, the calculations at 300 K show only small differences corresponding to shifts of approximately 1% of the total population. This is consistent with the high-temperature results for the unhydrated molecule reported in ref 24.

However, more substantial quantum effects are found in the hydrated clusters at 100 K. For the $n = 1$ and $n = 3$ clusters, we calculate a shift of approximately 10% of the total population from the GG′ conformer to the AG conformer. For the $n = 2$ cluster, a more dramatic quantum shift of approximately 30% is calculated, which changes the classical prediction of the GG′:AG population ratio from 4:1 to 1:1. The quantum effects in the conformer populations reported in Table 5 are larger than we have found in previous TPIMC calculations.

TABLE 3: Conformer Populations[a] for the Hydrated APE Conformers

	100 K				300 K			
APE + nH$_2$O	AG	AG′	GG	GG′	AG	AG′	GG	GG′
0H$_2$O	79.6(3)[b]	0.346(2)	20.0(3)	0.0	50.7(2)	16.29(5)	22.5(2)	0.910(8)
1H$_2$O	74(2)	0.34(3)	7.2(8)	18(2)	48.2(8)	16.6(2)	22.1(8)	2.3(1)
2H$_2$O	42(4)	5.4(5)	10(1)	41(4)	48.5(8)	17.5(2)	20.4(8)	3.2(1)
3H$_2$O	25(3)	4.7(6)	8(1)	62(5)	46.1(5)	18.3(1)	19.9(3)	4.7(1)
4H$_2$O	51(3)	21(3)	12(2)	15(3)	45(1)	19.2(5)	18(1)	5.3(5)

[a] Conformer populations reported in percentages. [b] Numbers in parentheses are the standard deviation in the last reported digit.

TABLE 4: Relative Standard Internal Energies[a] and Entropies[b] for the Hydrated APE Conformers

	$\Delta E°$				$\Delta S°$			
APE +nH$_2$O	AG	AG′	GG	GG′	AG	AG′	GG	GG′
0H$_2$O	0.0	5.33(1)	0.65(1)	12.3(1)[c]	0.0	7.87(5)	−3.79(8)	7.6(2)
1H$_2$O	0.0	6.0(2)	2.6(1)	−0.6(1)	0.0	5.7(4)	−4.6(8)	−29(1)
2H$_2$O	0.0	0.8(2)	−0.4(2)	−4.9(1)	0.0	3.1(8)	−3.1(1)	−39(1)
3H$_2$O	0.0	1.6(2)	−0.4(2)	−4.3(4)	0.0	−2(1)	−3(1)	−37(1)
4H$_2$O	0.0	−1.2(2)	0.3(3)	−1.0(2)	0.0	−4(2)	−5(4)	−35(3)

[a] $\Delta E°$ in kJ/mol. Calculated at 100 K. [b] $\Delta S°$ in J/(mol/K). Calculated at 300 K. [c] Because of insufficient sampling of this conformer at 100 K, the value calculated at 300 K is reported.

TABLE 5: Conformer Population Shifts Due to Quantum Effects[a]

	100 K				300 K			
APE + nH$_2$O	AG	AG′	GG	GG′	AG	AG′	GG	GG′
0H$_2$O	3.1(4)	0.12(1)	−3.2(4)	0(0)	−0.4(2)	0.59(6)	−0.7(2)	0.04(1)
1H$_2$O	9(2)	0.08(3)	0.0(8)	−10(2)	−1.2(8)	0.5(2)	−0.5(8)	−0.04(1)
2H$_2$O	24(4)	2.8(5)	2(1)	−32(4)	0.8(8)	0.7(2)	−1.0(8)	−0.5(1)
3H$_2$O	8(4)	2.3(7)	0(1)	−10(6)	0.1(6)	0.4(2)	−0.3(6)	−0.4(1)
4H$_2$O	−5(4)	0(4)	1(2)	4(4)	−2(1)	−0.8(6)	0(1)	0.6(5)

[a] Difference between quantum and classical TPIMC populations reported in percentages of the total population.

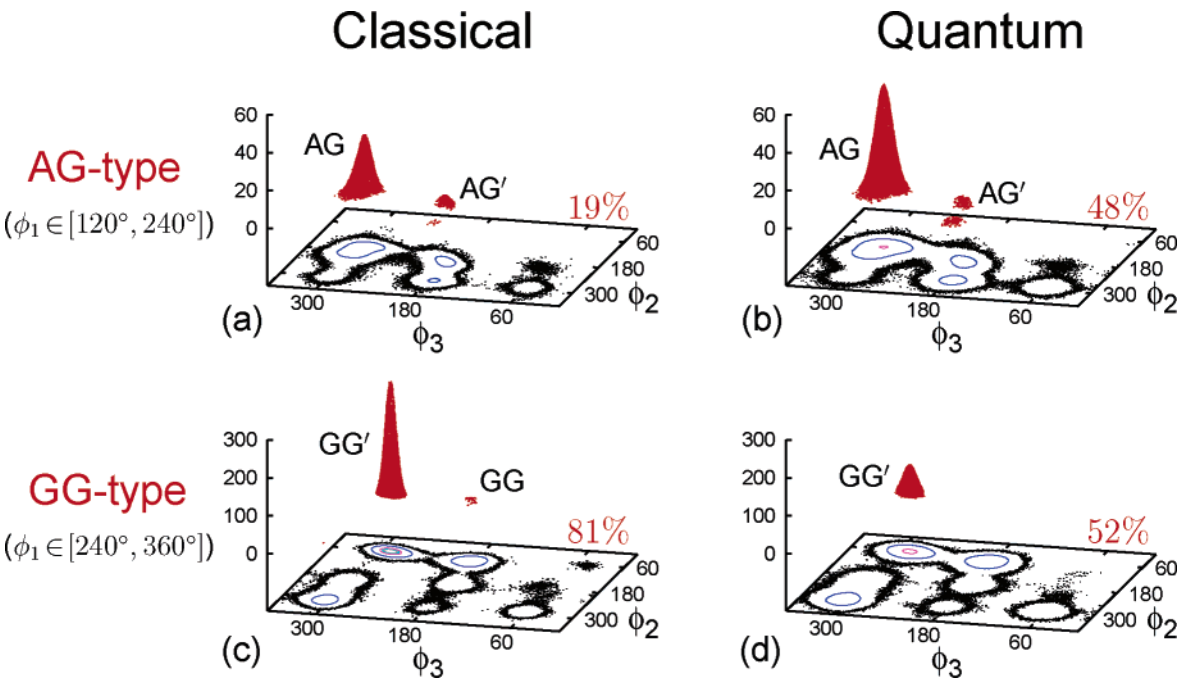

Figure 3. Probability distributions at 100 K for the APE+2H$_2$O cluster as a function of the −OH torsion ϕ_2 and the −NH$_2$ torsion ϕ_3. (a) Classical distribution for the AG-type conformers ($\phi_1 \in$ [120°,240°]). (b) Quantum distribution for the AG-type conformers. (c) Classical distribution for the GG-type conformers ($\phi_1 \in$ [240°,360°]). (d) Quantum distribution for the GG-type conformers. Numbers in red indicate the percentage of the total population represented by the corresponding distribution plot.

To study the large quantum effects at 100 K, we consider the $n = 2$ cluster in greater detail. Figure 3 presents torsional distributions for this system obtained from the classical TPIMC simulations (Figure 3a,c) and the quantum TPIMC simulations (Figure 3b,d). The plots for the AG-type conformers of the hydrated APE molecule (Figure 3a,b) were calculated by reducing the torsional distribution $\rho(\vec{\phi})$ by integrating over the entire range of the phenyl torsion $\phi_0 = [0°,360°]$ and a part of the range of the backbone C−C torsion $\phi_1 = [120°,240°]$. The result is a distribution function of the −OH torsion ϕ_2 and the −NH$_2$ torsion ϕ_3 which corresponds to the AG-type conformations (i.e., AG and AG′). Similarly, the GG-type distribution

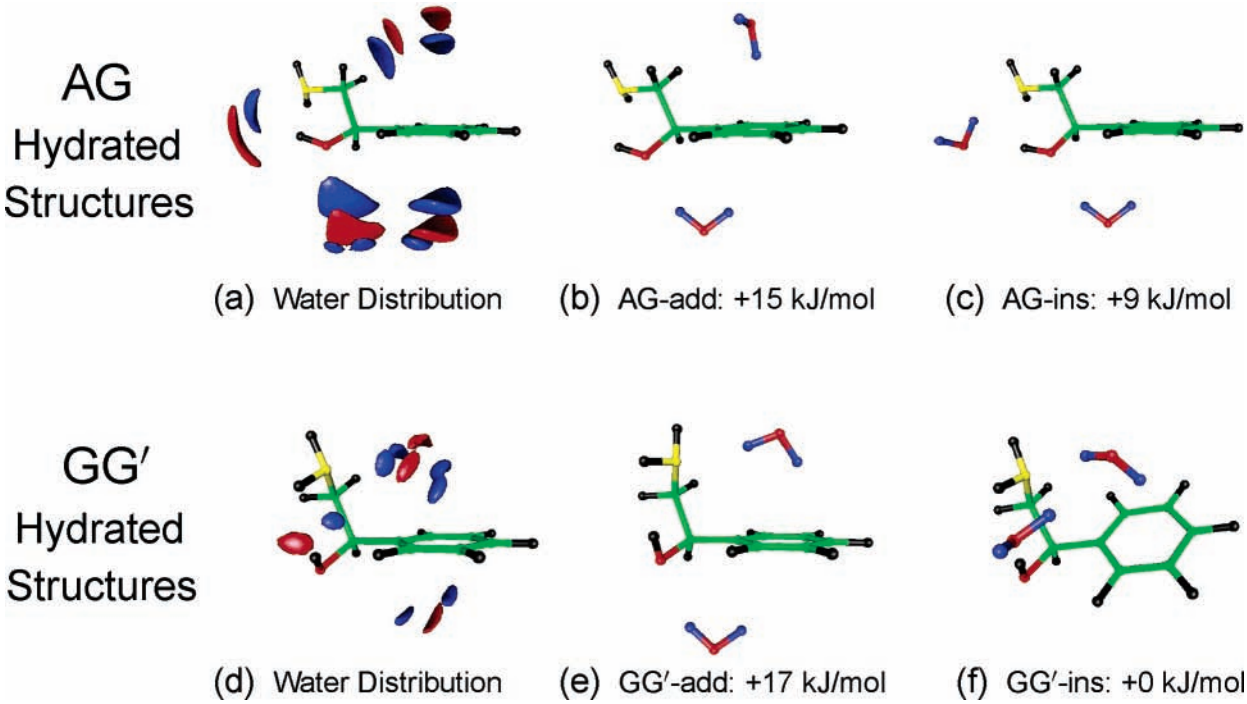

Figure 4. Hydrated structures for the APE + $2H_2O$ cluster. (a and d) Distribution of water molecules calculated at 100 K for the AG conformer and the GG conformer, respectively. Red surfaces indicate oxygen atom density; blue surfaces indicate hydrogen atom density. Hydrated structures, shown to the right of the distribution plots, are optimized subject to the internal constraints used in the simulation. MM3 potential energies reported.

plots were obtained by integrating $\rho(\vec{\phi})$ over $\phi_0 = [0°,360°]$ and $\phi_1 = [120°, 240°]$. The percentage of the total population represented in each distribution is reported in red; note that the populations of the AG-type conformers and the GG-type conformers sum to 100% in both the classical and quantum simulations.

Figure 3 reiterates the large quantum shift in the population of the $n = 2$ cluster from the GG′ conformer to the AG conformer. In the classical simulation, 80% of the total population is found in the GG-type conformations (Figure 3c). The torsional distribution is localized into a very narrow GG′ peak at $(\phi_2,\phi_3) = (60°,300°)$. This GG′ conformation remains the dominant feature in the corresponding quantum distribution (Figure 3d), but its magnitude is much diminished. In the distribution plots for the AG-type conformations (Figure 3a and b), both the classical and quantum distributions are dominated by a relatively broad AG conformation peak at $(\phi_2,\phi_3) = (180°,-300°)$.

In Figure 4, we explore the actual structures of the APE + $2H_2O$ cluster that give rise to the largest peaks in Figure 3. The distribution of the water molecules for the conformers of interest were calculated in the TPIMC simulations by integrating the Boltzmann probability distribution $\rho(\vec{\phi},\vec{r},\vec{\theta})$ over (1) the total translational motion of the cluster, (2) the total rotational motion of the cluster, and (3) the torsional ranges specific to the conformer of interest. The resulting conformer-specific distribution is a function of the relative position of the APE molecule and the water molecules. The distribution of water molecules corresponding to the AG conformer of the APE molecule is shown in Figure 4a; the water distribution obtained for the GG′ conformer is shown in Figure 4d. The red surfaces indicate the position of the oxygen atoms, and the blue surfaces indicate the position of the hydrogen atoms; for each conformer, the cutoffs for both the hydrogen and oxygen surfaces were set to the same value. The water distribution plots were obtained from the classical TPIMC simulations at 100 K and provide a clear indication of the preferred binding sites for the water molecules. It should be noted that parts a and d of Figure 4 correspond to the time-averaged distribution of *both* water molecules in the cluster; they do not provide any information about the relative position of the two water molecules at any given instant in time.

Figure 4a presents the distribution of water molecules for the AG conformer of the APE + $2H_2O$ cluster at 100 K; it provides a detailed picture of the hydrated structures that give rise to the large AG peak at $(\phi_2,\phi_3) = (180°,300°)$ in Figure 3a. It is clear from Figure 4a that the two water molecules bind to the APE molecule at five different sites: two sites are above the APE molecule, two are below, and one is at the tail of the APE molecule. In each case, a region of hydrogen (blue) density is seen between the APE molecule and a region of oxygen (red) density. In the binding sites below the molecule, a second region of hydrogen density is observed on the far side of the oxygen density, indicating the orientation of the water molecule. However, at the other sites, the position of the second hydrogen atom either coincides with that of the first or is too delocalized to be observed with the employed value of the surface cutoff.

The ability of the AG conformer to accommodate water-binding at so many sites most likely contributes to its large entropy, as reported in Table 4. It is seen in Figure 4d that a smaller number of binding sites are available for the GG′ conformer: one below the APE molecule, one at the tail, and one (perhaps two) above the molecule. The GG′ conformer was seen in Table 4 to have a much lower relative entropy.

It is useful to determine the specific structures of APE + $2H_2O$ that give rise to the water distribution plots in Figure 4a,d. A search of the potential energy surface (subject to the internal constraints employed in the simulations) revealed numerous local minima, some of which are shown to the right of the corresponding water distribution plots.

The lowest-energy hydrated structure found for the AG conformer is the AG-ins structure seen in Figure 4c. In this structure, a water molecule occupies the binding site below the APE molecule, aligned with the intramolecular hydrogen bond between the $-$OH group and $-NH_2$ in the tail of the APE

TABLE 6: Relative Harmonic Zero Point Energy[a] for the Structures of APE + $2H_2O$ in Figure 4

hydrated structure	relative harmonic ZPE
AG-add	0.0
AG-ins	2.7
GG′-add	3.9
GG′-ins	8.3

[a] ZPE in kJ/mol. Calculated using the MM3 harmonic normal mode vibrational frequencies for the optimized hydrated structures.

molecule; the other water molecule is partially inserted into this intramolecular hydrogen bond. A second AG hydrated structure, AG-add in Figure 4b, is found at somewhat higher energy. In this structure, one of the water molecule occupies a binding site above the APE molecule, forming a hydrogen bond with the phenyl ring, and the other occupies a binding site below the APE molecule, aligned with the intramolecular hydrogen bond.

Similar hydrated structures are found for the GG′ conformer. The GG′-add structure in Figure 4e is found to be similar in energy to the AG′-add structure and also exhibits water molecules in the binding sites above and below the APE molecule. However, the GG′-ins structure in Figure 4f is particularly interesting. It is markedly lower in energy than any of the other hydrated structures, and it exhibits an intricate hydrogen-bonding network that involves both water molecules, both polar groups of the APE molecule, and the phenyl ring. As is seen in Figure 4f, the oxygen atom of one of the water molecules in the GG′-ins structure receives hydrogen bonds from both the $-OH$ and $-NH_2$ groups of the APE molecule. Simultaneously, this water molecule donates a hydrogen bond to the other water molecule, which is donating hydrogen bonds to the $-NH_2$ group and the phenyl group on the APE molecule.

The low energy and complicated hydrogen-bonding network of the GG′-ins structure together explain the sharpness of the GG′ peak in the classical torsional distribution in Figure 3c. The energetic stability of the GG′-ins structure ensures that it is populated in the classical distribution (as is confirmed in the water distribution plots in Figure 4d), but the complicated hydrogen-bonding network is likely to be disrupted by only small changes in the torsional degrees of freedom. The AG hydrated structures exhibit hydrogen bonding networks that are less sensitive to small changes in the torsional coordinates; the greater flexibility gives rise to the broader peaks in Figure 3a.

These factors also suggest a reason for the large quantum effect in the relative population of the AG and GG′ conformers (Figure 3 and Table 5). The complicated hydrogen-bonding network of the GG′ conformer (and sharpness of the GG′ peak in Figure 3c) suggests that small changes in the internal coordinates of the GG′-ins structure corresponds to large changes in its potential energy. This indicates a high vibrational force constant for the internal modes and a large amount of quantum zero point energy for the structure. Structures with more internal flexibility, such as the hydrated AG structures, might be expected to have lower vibrational force constants and less quantum zero point energy. This interpretation is clearly supported by the harmonic vibrational zero point energies for the various structures reported in Table 6. The comparatively high quantum zero point energies of the GG′ hydrated structures (particularly that of the GG′-ins structure) appear to be primarily responsible for the calculated shift in the relative populations of the AG and GG′ conformers seen in Figure 3 and Table 5. Similar shifts in conformer population due to quantum zero point energy have been found in diffusion Monte Carlo studies of small protonated water clusters.[26]

3. Comparison with Experiment. Macleod et al. have studied the hydrated APE clusters (APE + nH_2O, $n = 1-4$) using a combination of resonant two-photon ionization spectroscopy and time-of-flight mass spectrometry, as well as infrared (IR) ion-dip spectroscopy.[51] These gas-phase experiments (a) isolate hydrated APE clusters with a particular hydration number n from a molecular beam, (b) determine the number of structures with that hydration number found in the beam, and (c) isolate each of these individual structures and record its IR spectrum. The result is direct geometric information (in the form of an IR spectrum) regarding the individual structures present in the molecular beam. The experiments are performed by initially preparing the hydrated clusters in an oven before allowing them to undergo collisional cooling in the molecular beam for spectroscopic analysis.

An interesting result from these experiments is that, for each hydration number, only one or two structures were observed in the molecular beam.[51] Given the high temperature of the oven (353 K) and the large number of low-energy local minima reported for the ab initio potential energy surface, a much larger number of observed structures might have been expected. To explain this result, the authors noted that structures in the oven experience collisions in the molecular beam that can change their geometry.[51] In some systems, the collisional cooling process gives rise to final distributions that deviate substantially from thermal equilibrium.[33,52−58]

Because the TPIMC method only provides information regarding the equilibrium distribution of the hydrated clusters, it is clear that care must be taken in comparing our calculations with the results from ref 51. Nonetheless, qualitative comparisons provide encouraging agreement.

In every case, the experimental spectra were assigned to hydrated structures in which the APE molecule is in an AG-type conformation (with $\phi_1 \in [120°,240°]$).[51] The structural assignments were based on the comparison of measured and calculated IR spectra (including, in some cases, the analysis of rotational band contours), as well as the calculated relative energy of candidate hydrated structures using ab initio methods. Even for the $n = 1$ hydrated cluster, in which a GG-type structure was calculated to be the global minimum of the potential energy surface, AG-type structures were found to be in better agreement with the observed spectra.

This result is consistent with the calculations presented in Tables 3 and 4. In Table 3, the combined population of the AG-type structures ($\phi_1 \in [120°,240°]$) at 300 K exceeds that of the GG-type structure ($\phi_1 \in [240°,360°]$) by a factor of 3, regardless of the number of hydrating water molecules. The entropic favorability of the AG-type conformers (Table 4) ensures that these structures will remain strongly favored at the higher experimental temperature of 353 K, which was confirmed by explicit calculations on the $n = 0$ and $n = 1$ clusters. The predominance of AG-type structures at thermal equilibrium in the oven, as predicted by our calculations, supports the fact that AG-type structures are more readily detected in the experiment.

Incidentally, our explanation for the presence of AG-type structures in the experimental spectra of the $n = 1$ cluster differs somewhat from that provided in ref 51. Macleod et al. calculated that a GG-type structure was the global minimum of the potential energy surface and estimated that the relative entropy of the AG-type and GG-type structures was zero; it follows that GG-type structures would remain heavily populated in the oven of the experiment. They suggested that the absence of these GG-type structures from the measured spectra was due entirely to structural interconversion in the molecular beam. Although

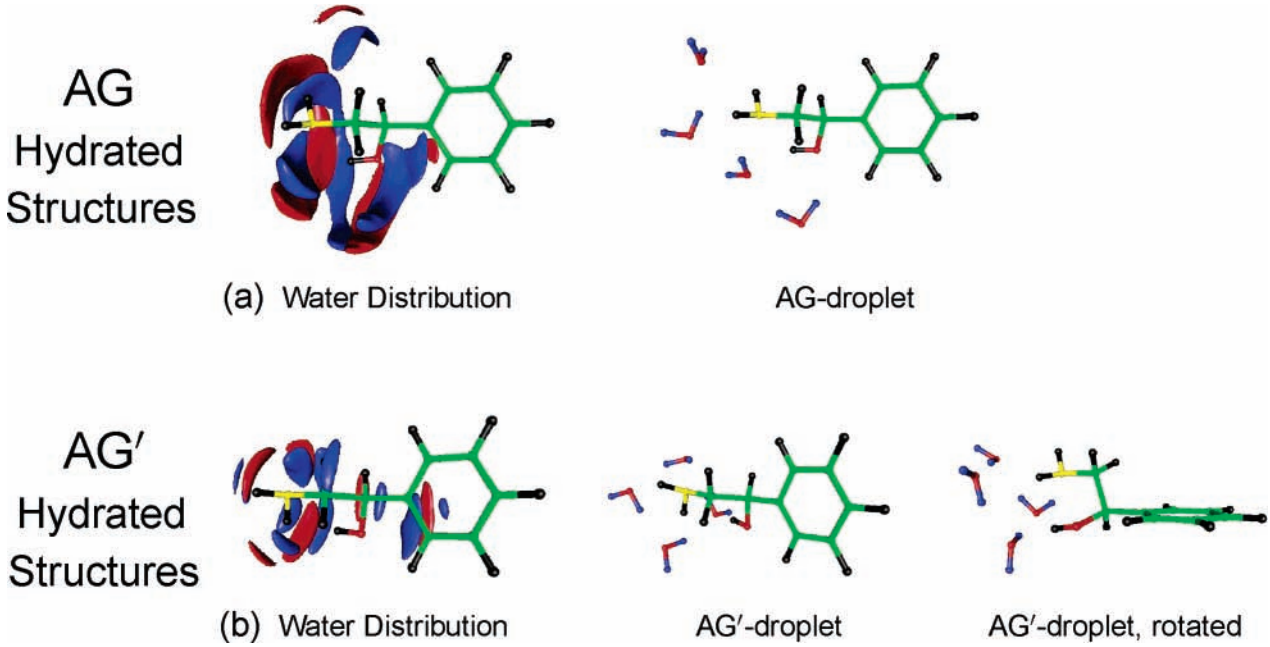

Figure 5. Hydrated structures for the APE + $4H_2O$ cluster. Distribution of water molecules calculated at 100 K for (a) the AG conformer and (b) the AG′ conformer. Red surfaces indicate oxygen atom density; blue surfaces indicate hydrogen atom density. Representative hydrated structures are shown to the right of the distribution plots.

we agree that GG-type → AG-type interconversion in the molecular beam is possible for the hydrated clusters, we have shown that the AG-type conformers are in fact strongly favored by entropy, which means that the original population of structures in the oven *already* favors the experimental detection of the AG-type structures.

Another qualitative comparison between the experimental results and our calculations can be made for the $n = 4$ hydrated cluster. Macleod et al. observed that the IR spectrum measured for this cluster was "quite distinctive and considerably more complex" than those for the smaller clusters.[51] They associated this complexity with the formation of a four-molecule water "droplet" at the flexible tail of the APE molecule. Our calculations agree that the potential energy surface of the $n = 4$ cluster is different in character from those of the smaller clusters. The relative conformer internal energies in Table 4 change substantially with the addition of a fourth water molecule, giving rise to the dramatic shift in conformer population seen in the left column of Figure 2. Furthermore, in Figure 5, we present the water distributions at 100 K for the most stable AG and AG′ conformers of the $n = 4$ cluster, which clearly show the formation of a water droplet at the tail of the APE molecule. The alternating red and blue regions indicate an assembly of water molecules interacting via hydrogen bonds. For illustrative purposes, minimized hydrated structures of the $n = 4$ cluster are shown to the right of each distribution plot in Figure 5.

V. Conclusions

An extended version of the TPIMC method has been developed and shown to be useful for exploring the hydration of flexible biomolecules. APE + nH_2O clusters with $n = 0-4$ were studied at 100 and 300 K using both classical and quantum TPIMC simulations. Only at the lower temperature was the hydration number n found to impact the torsional distribution of the APE molecule. This was shown to be a result of the temperature-dependent balance between the internal energy and entropy contributions to the relative conformer free energies. Furthermore, at 100 K, large quantum effects were observed in the calculated conformer populations. A particularly large quantum shift of 30% of the total population was calculated for the APE + $2H_2O$ cluster, which was explained in terms of the relative zero point energy of the lowest-energy hydrated structures for this cluster. Finally, qualitative agreement was found between the reported calculations and recent spectroscopy experiments on the hydrated clusters of APE, including an entropically driven preference for the formation of AG-type hydrated structures and the formation of a water "droplet" in the APE + $4H_2O$ cluster.

Acknowledgment. T.F.M. and D.C.C. acknowledge fellowships from the National Science Foundation and the Leverhulme Trust, respectively. The authors also thank Guy Grant and Christopher Baker for many insightful conversations.

References and Notes

(1) See, for example: *Phys. Chem. Chem. Phys.* **2004**, *6*, (10). Special issue on bio-active molecules in the gas phase.
(2) See, for example: *Mol. Phys.* **2005**, *103*, (11−13). Special issue in honor of Prof. John P. Simons.
(3) Weaver, R. F. *Molecular Biology*, 2nd ed.; McGraw-Hill: New York, 2002.
(4) Lodish, H.; Berk, A.; Matsudaira, P.; Kaiser, C. A.; Krieger, M.; Scott, M. P.; Zipursky, L.; Darnell, J. *Molecular Cell Biology*, 5th ed.; Freeman: New York, 2003.
(5) Zwier, T. S. *J. Phys. Chem. A* **2001**, *105*, 8827.
(6) Robertson, E. G.; Simons, J. P. *Phys. Chem. Chem. Phys.* **2001**, *3*, 1.
(7) Snoek, L. C.; Robertson, E. G.; Kroemer, R. T.; Simons, J. P. *Chem. Phys. Lett.* **2000**, *321*, 49.
(8) Graham, R. J.; Kroemer, R. T.; Mons, M.; Robertson, E. G.; Snoek, L. C.; Simons, J. P. *J. Phys. Chem. A* **1999**, *103*, 9706.
(9) Brauer, B.; Chaban, G. M.; Gerber, R. B. *Phys. Chem. Chem. Phys.* **2004**, *6*, 2543.
(10) van Mourik, T.; Früchtl, H. A. *Mol. Phys.* **2005**, *103*, 1641.
(11) Levy, D. H. *Science* **1981**, *214*, 263.
(12) Zwier, T. S. *Annu. Rev. Phys. Chem.* **1996**, *47*, 205.
(13) Simons, J. P. *C. R. Chim.* **2003**, *6*, 17.
(14) Weinkauf, R.; Schermann, J. P.; de Vries, M. S.; Kleinermanns, K. *Eur. Phys. J. D* **2002**, *20*, 309.
(15) Dian, B. C.; Longarte, A.; Zwier, T. S. *Science* **2002**, *296*, 2369.
(16) Dong, F.; Miller, R. E. *Science* **2002**, *298*, 1227.

(17) Clarkson, J. R.; Baquero, E.; Shubert, V. A.; Myshakin, E. M.; Jordan, K. D.; Zwier, T. S. *Science* **2005**, *307*, 1443.
(18) Pitzer, K. S.; Gwinn, W. D. *J. Chem. Phys.* **1942**, *10*, 428.
(19) Glaesemann, K. R.; Fried, L. E. *J. Chem. Phys.* **2003**, *118*, 1596.
(20) Glaesemann, K. R.; Fried, L. E. *J. Chem. Phys.* **2005**, *123*, 034103.
(21) Tachikawa, M.; Shiga, M. *J. Chem. Phys.* **2004**, *121*, 5985.
(22) Lynch, V. A.; Mielke, S. L.; Truhlar, D. G. *J. Chem. Phys.* **2004**, *121*, 5148.
(23) Miller, T. F.; III; Clary, D. C. *Mol. Phys.* **2005**, *103*, 1573.
(24) Miller, T. F.; III; Clary, D. C. *J. Phys. Chem. B* **2004**, *108*, 2484.
(25) Miller, T. F.; III; Clary, D. C. *Phys. Chem. Chem. Phys.* **2004**, *6*, 2563.
(26) Mella, M.; Clary, D. C. *J. Chem. Phys.* **2003**, *119*, 10048.
(27) Mella, M.; Kuo, J. L.; Clary, D. C.; Klein, M. L. *Phys. Chem. Chem. Phys.* **2005**, *7*, 2324.
(28) Clary, D. C.; Benoit, D. M.; van Mourik, T. *Acc. Chem. Res.* **2000**, *33*, 441.
(29) van Mourik, T.; Benoit, D. M.; Price, S. L.; Clary, D. C. *Phys. Chem. Chem. Phys.* **2000**, *2*, 1281.
(30) Moskowitz, J. W.; Bačić, Z.; Sarsa, A.; Schmidt, K. E. *J. Chem. Phys.* **2001**, *114*, 10294.
(31) Miller, T. F.; III; Clary, D. C. *J. Chem. Phys.* **2002**, *116*, 8262.
(32) Miller, T. F.; III; Clary, D. C. *J. Chem. Phys.* **2003**, *119*, 68.
(33) Miller, T. F.; III; Clary, D. C.; Meijer, A. J. H. M. *J. Chem. Phys.* **2005**, *122*, 244323.
(34) Sturdy, Y. K.; Skylaris, C. K.; Clary, D. C. *J. Phys. Chem. B*, in press.
(35) Main, B. G. In *Comprehensive Medicinal Chemistry Vol. 3: Membranes and Receptors*; Hansch, C., Ed.; Pergamon Press: Oxford, England, 1990; p 187.
(36) Waxham, M. N. In *Fundamental Neuroscience*; Ziglund, M. J., et al., Eds.; Academic Press: London, 2003, p 225.
(37) Gouldson, P. R.; Snell, C. R.; Reynolds, C. A. *J. Med. Chem.* **1997**, *40*, 3871.
(38) Feynman, R. P.; Hibbs, A. R. *Quantum Mechanics and Path Integrals*; McGraw-Hill: New York, 1965.
(39) Chandler, D.; Wolynes, P. G. *J. Chem. Phys.* **1981**, *74*, 4078.
(40) Marx, D.; Muser, M. H. *J. Phys.: Condens. Matter* **1999**, *11*, R117.
(41) Cao, J. *Phys. Rev. E* **1994**, *49*, 882.
(42) Frenkel, D.; Smit, B. *Understanding Molecular Simulation*; Academic Press: New York, 2002.
(43) Kuharski, R. A.; Rossky, P. J. *J. Chem. Phys.* **1985**, *82*, 5164.
(44) Allinger, N. L.; Yuh, Y. H.; Lii, J.-H. *J. Am. Chem. Soc.* **1989**, *111*, 8551.
(45) Scheiner, S. *Annu. Rev. Phys. Chem.* **1994**, *45*, 23.
(46) Lee, J. K.; Barker, J. A.; Abraham, F. F. *J. Chem. Phys.* **1973**, *58*, 3166.
(47) Freeman, D. L.; Doll, J. D. *Adv. Chem. Phys. B* **1988**, *70*, 139.
(48) Freeman, D. L.; Doll, J. D. *J. Phys. Chem.* **1985**, *82*, 462.
(49) Barker, J. A. *J. Chem. Phys.* **1979**, *70*, 2914.
(50) DeVoe, H. In *Structure and Stability of Biological Molecules*; Timasheff, S. N., Fasman, G. D., Eds.; Marcel Dekker: New York, 1969.
(51) Macleod, N. A.; Robertson, E. G.; Simons, J. P. *Mol. Phys.* **2003**, *101*, 2199.
(52) Ruoff, R. S.; Klots, T. D.; Emilsson, T.; Gutowsky, H. S. *J. Chem. Phys.* **1990**, *93*, 3142.
(53) Godfrey, P. D.; Brown, R. D.; Rodgers, F. M. *J. Mol. Struct.* **1996**, *376*, 65.
(54) Godfrey, P. D.; Brown, R. D. *J. Am. Chem. Soc.* **1998**, *120*, 10724.
(55) Florio, G. M.; Christie, R. A.; Jordan, K. D.; Zwier, T. S. *J. Am. Chem. Soc.* **2002**, *124*, 10236.
(56) Butz, P.; Kroemer, R. T.; Macleod, N. A.; Simons, J. P. *Phys. Chem. Chem. Phys.* **2002**, *4*, 3566.
(57) Bastida, A.; Zúñiga, J.; Requena, A.; Miguel, B.; Alberto Beswick, J.; Vigue, J.; Halberstadt, N. *J. Chem. Phys.* **2002**, *116*, 1944.
(58) Evans, D. A.; Wales, D. J.; Dian, B. C.; Zwier, T. S. *J. Chem. Phys.* **2004**, *120*, 148.